A Fluorescent Sensor of the Phosphorylation State of Nucleoside Diphosphate Kinase and Its Use To Monitor Nucleoside Diphosphate Concentrations in Real Time†

Martin Brune, John E. T. Corrie, and Martin R. Webb*

National Institute for Medical Research, Mill Hill, London NW7 1AA, U.K.

Received October 26, 2000; Revised Manuscript Received February 9, 2001

ABSTRACT: A sensor for purine nucleoside diphosphates in solution based on nucleoside diphosphate kinase (NDPK) has been developed. A single cysteine was introduced into the protein and labeled with the environmentally sensitive fluorophore, *N*-[2-(iodoacetamido)ethyl]-7-diethylaminocoumarin-3-carboxamide. The resultant molecule shows a 4-fold fluorescence increase when phosphorylated on His117; this phosphorylation is on the normal reaction pathway of the enzyme. The emission maximum of the phosphoenzyme is at 475 nm, with maximum excitation at 430 nm. The fluorescent phosphorylated NDPK is used to measure the amount of ADP and the unphosphorylated to measure ATP. The labeled protein is phosphorylated to >90%, and the resultant molecule is stable on ice or can be stored at −80 °C. The fluorescence responds to the fraction of protein phosphorylated and so to the equilibrium between ADP plus NDPK∼P and ATP plus NDPK. In effect, the sensor measures the ADP/ATP concentration ratio. The enzyme has a broad specificity for the purine of the nucleotides, so the sensor also can measure GDP/GTP ratios. The fluorescence and kinetic properties of the labeled protein are described. The binding rate constants of nucleotides are $\sim 10^5$ M^{-1} s^{-1}, and the fluorescence change is at >200 s^{-1} when the ADP concentration is >1 mM. Results are presented with two well-defined systems, namely, the kinetics of ADP release from myosin subfragment 1 and GDP release from the small G protein, human rho. The results obtained with this novel sensor agree with those from alternate methods and demonstrate the applicability for following micromolar changes in nucleoside diphosphate in real time.

Muscle contraction is an example of a system where there is a precise relationship between a physiological response, contraction in this case, and biochemical events, the ATPase cycle in this case. Assessing biochemical processes such as the release of reaction products in such a system is essential to understanding the relationship of such reactions to physiological observations. Several techniques have been tried more or less successfully to obtain the high time resolution necessary to assess parts of the actomyosin ATPase cycle that correspond to changes in the mechanical properties (reviewed in ref *1*). In particular, the release of products from the ATPase activity in this system is intimately linked with the mechanical changes. We have taken an approach to create fluorescent sensors specifically for monitoring the release of products within a single muscle fiber. Requirements for such sensors include a large signal change over a range of several hundred micromolar product concentrations and a rapid response, i.e., on a millisecond time scale.

Previously, we developed a fluorescent sensor (MDCC-PBP)[1] for another reaction product, inorganic phosphate (P_i) (*2*−*4*). It consists of the phosphate binding protein (PBP) of *Escherichia coli*, labeled with a coumarin fluorophore at a single cysteine that was introduced by site-directed mutagenesis. Upon binding of P_i, there is a large fluorescence increase and the sensor is sensitive down to nanomolar concentrations of P_i. Because of the ubiquity of P_i as a reaction product from ATPases and GTPases, the sensor has been used to assess P_i release for several different systems (*2*, *5*−*8*).

Here we describe a fluorophore-labeled protein for measuring ADP and GDP concentrations directly under physiological conditions. Furthermore, it can monitor changes in concentrations in real time, as when the diphosphates are released following triphosphate hydrolysis by ATPases and GTPases. A major challenge was to find a system that could measure the amount of diphosphate, but be insensitive to triphosphates, which are present as the substrates for these enzymes.

The diphosphate sensor is based on nucleoside diphosphate kinase (NDPK), a ubiquitous enzyme that catalyzes the transfer of the γ-phosphate group of one purine nucleoside

† This work was supported by the Medical Research Council, U.K.

* To whom correspondence should be addressed. Telephone: (44) 20 8959 3666. Fax: (44) 20 8906 4477. E-mail: mwebb@nimr.mrc.ac.uk.

[1] Abbreviations: NDPK, nucleoside diphosphate kinase; $NDPK^{D112C}$, D112C mutant of NDPK; DCC-NDPK, D112C mutant of NDPK labeled with IDCC; DCC-NDPK∼P, DCC-NDPK phosphorylated at His117; IDCC, *N*-[2-(iodoacetamido)ethyl]-7-diethylaminocoumarin-3-carboxamide; MDCC, *N*-[2-(1-maleimidyl)ethyl]-7-diethylaminocoumarin-3-carboxamide; CPM, 7-(diethylamino)-3-[4′-(1-maleimidyl)-phenyl]-4-methylcoumarin; Acrylodan, 6-acryloyl-2-(dimethylamino)-naphthalene; Coumarin 314, ethyl 2,3,6,7-tetrahydro-11-oxo-1*H*,5*H*,11*H*[1]-benzopyrano[6,7,8-*ij*]quinolizine-10-carboxylate; PBP, phosphate binding protein; MDCC-PBP, A197C mutant of PBP labeled with MDCC.

10.1021/bi002484h CCC: $20.00
Published on Web 03/29/2001

triphosphate (N_1TP) onto another purine nucleoside diphosphate (N_2DP) with very little specificity for the base. The reaction consists of two phosphotransfers with a phosphohistidine intermediate, which is relatively stable.

$$N_1TP + E \rightleftharpoons E{\sim}P + N_1DP \quad (1)$$

$$N_2DP + E{\sim}P \rightleftharpoons E + N_2TP \quad (2)$$

For a summary of enzymatic properties, see ref *9*. NDPK is fully active as an oligomer, most often a tetramer or hexamer depending on the source, with no cooperativity between the subunits. Each monomer contains only one nucleotide binding site, so the donor nucleotide binds, reacts, and dissociates before the acceptor nucleotide binds. These partial reactions have been studied independently (*10*). The main physiological role of NDPK is to equilibrate the nucleotide pool in cells. In humans, however, a single point mutation of NDPK isoform A has been found in tumor cells (*11*) and NDPK A is involved in tumor metastasis (for a review, see ref *12*). In bacteria, NDPK plays a role in the virulence of respiratory tract pathogens (*13*).

Three-dimensional crystal structures of NDPK from several sources have been determined with or without nucleotides bound (*14*−*17*). There are only small conformational changes in the structures upon nucleotide binding. The catalytic site itself consists of the same characteristic fold in all NDPK structures, but is distinctly different from that of other kinases and purine nucleotide binding proteins (*16*). There are only few contacts between the protein and the base of the bound nucleotide, reflecting the low base specificity of the enzyme. The overall level of homology between NDPKs is high, with 30% identical amino acids among all NDPKs and 57% between the bacterial enzymes of *E. coli* and *Myxococcus xanthus* (*18*).

NDPK from *M. xanthus* was chosen as the basis for the fluorescent diphosphate sensor for the following reasons. Its gene has been cloned into *E. coli*, and the protein has been characterized (*19*, *20*), including by crystallography. This enzyme is a tetramer of four identical 16 kDa subunits (*15*) and contains no cysteines. To provide a reactive site for covalent attachment of a fluorophore, single cysteine residues were introduced at defined positions in the molecule by site-directed mutagenesis. Various positions were chosen on the basis of the crystal structure and generally were located at the outer edge of the nucleotide binding cleft. Several environmentally sensitive fluorophores were attached to these sites, and the ability of each label-mutant combination to report changes in the nucleotide binding site was tested to obtain the optimal combination of position and fluorophore.

The measurement of the amount of diphosphate by the sensor makes use of the dephosphorylation partial reaction (eq 2). By screening the combinations of labeled NDPKs for differences in fluorescence in the presence of either ATP or ADP, we found combinations in which the fluorescence intensity is sensitive to dephosphorylation. The diphosphate sensor shows a large change in the fluorescence signal when phosphate is transferred from the phosphoenzyme to ADP, whereas no signal change occurs when ATP is added to the phosphoenzyme. Because the substrate specificity of NDPK is low, there is no discrimination between GDP and ADP. The sensor can also monitor GDP, thereby increasing its applicability to a wide variety of systems where ADP or GDP is a product. This includes ATPases, GTPases, and kinases.

The applicability of the final fluorescent diphosphate sensor was demonstrated using two reactions. First, the kinetics of ADP release from subfragment 1, the enzymatically active subunit of myosin, were measured in solution. Second, GDP release from the small GTPase rho was assessed. Under normal conditions, guanine nucleotides form a tight complex with rho and both GTP hydrolysis and product release are slow. There is a net release of bound GDP from this active site only when a free nucleotide such as GTP is present to replace it.

EXPERIMENTAL PROCEDURES

Materials. E. coli strains TG1 (*21*) and DH5α (*22*) were used for mutagenesis and general cloning purposes. BL21 from Novagen was used for expression and overproduction of NDPK proteins. Plasmid pJM5C2A containing the *M. xanthus ndk* gene was provided by R. Williams (Cambridge University, Cambridge, U.K.). Recombinant rho protein was provided by J. Hutchinson (National Institute for Medical Research). Myosin subfragment 1 was prepared as described previously (*23*). Other enzymes and biochemicals were from Sigma, Boehringer, New England Biolabs, Bio-Rad, Amersham, or Stratagene. Fluorescent labeling reagents were obtained from Molecular Probes or synthesized (*24*).

Cloning and Mutagenesis. Site-directed mutagenesis was carried out using either the phosphorothioate-based kit (*25*) (Amersham) or the PCR-based QuikChange kit from Stratagene. For the former, the 0.8 kb *Hin*dIII−*Eco*RI fragment of pJM5C2A was ligated with M13mp19, and the resulting recombinant clones were used to provide single-stranded DNA templates for the mutagenesis reaction. For expression, the mutated *ndk* genes were cloned back into pJM5C2A in the same way as described above. Alternatively, the 0.7 kb *Bst*XI−*Eco*RI fragment of the M13 constructs (and of pJM5C2A as a wild-type *ndk* control) was ligated into a modified version of the expression vector pRSetA from Invitrogen, whose coding sequence for a histidine tag fused to the N-terminus of NDPK had been removed. The recombinant plasmid containing wild-type *ndk* was used as a template in the QuikChange mutagenesis method. General molecular biology techniques were carried out as described by Sambrook et al. (*26*).

Expression of the ndk Gene and Purification of NDPK. Expression of *ndk* in *E. coli* generally was more reliable from clones containing the pRSet constructs than from clones based on pJM5C2A, and therefore, the former were exclusively used for large-scale (4 L of culture medium) preparations. The following protocol describes the expression from pRSndk4 and the subsequent purification of $NDPK^{D112C}$, the mutant that was used in the fluorescence studies.

For *ndk* expression in *E. coli*, better yields were obtained using freshly transformed cells. Calcium-competent BL21 cells (200 μL) were incubated with pRSndk4 plasmid DNA (2 ng) for 30 min on ice. Half of this mixture was then spread onto a LB agar plate containing 0.1 mg/mL ampicillin and the plate incubated overnight at 37 °C. Typically, the plate contained 50−100 colonies. LB medium (100 mL), containing 0.1 mg/mL ampicillin, was inoculated with 2−3 colonies from the plate, and the colonies were grown for 9 h at 37

°C until the cells had just entered the stationary phase. For the main culture, 8 × 500 mL of LB with ampicillin was inoculated with 10 mL each of this starter culture and incubated at 37 °C for 6 h, after which time the cells had reached an OD^{595} of 0.38 cm^{-1}. At this point, 0.5 mM isopropyl thiogalactopyranoside was added to each flask, and the cells were grown for a further 16 h. Cells were harvested by centrifugation for 20 min in a Beckman L2 centrifuge at 3800 rpm and 20 °C. The pellet was resuspended in 100 mL of 20 mM Tris-HCl (pH 8.2) and 1 mM EDTA and stored at −80 °C.

One-third (∼35 mL) of the frozen cell suspension was lysed by thawing slowly from −80 °C and then sonicating. The cell suspension was then ultracentrifuged (Beckman L70 centrifuge, 45 Ti rotor, 1 h, 40 000 rpm, 4 °C).

Mutant NDPK was purified as follows with all steps at 4 °C. The supernatant was diluted to 200 mL in 20 mM Tris-HCl (pH 8.2), 1 mM EDTA, and 10 mM dithiothreitol and loaded onto an ion exchange column (120 mL) of Q-Sepharose (Pharmacia) at a flow rate of 2 mL/min. The column was washed with 1 volume of the same buffer and then eluted with a linear gradient (500 mL) from 0 to 0.3 M NaCl in this buffer at a rate of 1 mL/min. The bulk of NDPK (∼80%) was eluted without retention, and the remainder eluted at ∼100 mM NaCl. Both protein fractions were subsequently purified in the same way, but kept and stored separately. There is no apparent functional difference in activity between the two pools, but all the data were obtained with the flow-through protein.

After concentration using an ultrafiltration pressure cell with a YM10 membrane (Amicon), the eluate was purified on a gel filtration column (500 mL) of G-100 Sepharose (Pharmacia) in the same buffer as before, but without DTT, at a rate of 1 mL/min. Both fractions of NDPK coeluted from the Q-Sepharose column with poly- and oligonucleotides. Some NDPKs have been reported to bind DNA (*27*, *28*), and it could be that such a weak interaction causes the unusual elution pattern. The protein was separated from DNA by this subsequent gel filtration. Fractions containing NDPK were pooled and concentrated as before.

Protein concentrations were measured by UV absorbance spectroscopy, using a calculated extinction coefficient of 5180 M^{-1} cm^{-1} at 280 nm (*29*), and by the colorimetric Bio-Rad protein assay using bovine serum albumin as the standard. The final NDPK solution was stored at −80 °C. Mass spectrometry data showed that the purified protein was a single species with a molecular mass of 15993 ± 1 Da, matching the calculated molecular mass of the mutated *M. xanthus* enzyme minus the N-terminal methionine which is missing from this protein when it is produced in *E. coli* (*15*). The total yield of purified $NDPK^{D112C}$ from a 4 L cell culture was ∼300 mg.

E. coli's own NDPK is also expressed during induction, albeit at much lower levels than the *M. xanthus* gene. It is highly homologous to *M. xanthus* NDPK, has a similar molecular mass, and is also a tetramer (*30*). However, *E. coli* NDPK is eluted from the ion exchange column as a smaller, separate peak at a higher ionic strength than $NDPK^{D112C}$ and so is not present in the final *M. xanthus* NDPK pool.

Fluorescence Labeling. $NDPK^{D112C}$ was incubated with a 2.5-fold molar ratio of IDCC in 50 mM Tris-HCl (pH 8.1) for 1 h at 37 °C. Typically, the volume was 3 mL and the $NDPK^{D112C}$ concentration 150 μM, and the following protocol is based on this amount. After incubation, the solution was filtered through a 0.2 μm Acrodisc filter (Gelman) and loaded onto a PD10 desalting column (Pharmacia) equilibrated in 10 mM Tris-HCl (pH 8.0) and 1 mM EDTA at 20 °C. The eluate (∼6 mL) containing the labeled protein (DCC-NDPK) was further purified on an ion exchange column (25 mL) of Q-Sepharose equilibrated in the same buffer as above and with a linear gradient (200 mL) of 0 to 0.1 M NaCl at 4 °C. The labeled protein was not retained on the column and was concentrated in the same way as unlabeled NDPK. The concentration of the labeled protein was determined by the Bio-Rad assay described above and by absorbance spectroscopy. The coumarin extinction coefficient is 44 800 M^{-1} cm^{-1} at 430 nm [assuming it is the same as that of IDCC (*24*)], and the protein absorbance was corrected for the coumarin extinction coefficient at 280 nm (7470 M^{-1} cm^{-1}). The yield after labeling and purification was ∼65%.

To screen the fluorescence properties of different mutant-fluorophore combinations, labeling was performed on a smaller scale with 50−100 μM protein in a volume of 100−200 μL. All other conditions were as described above, except there was no filtration or Q-Sepharose column. Eluates from the PD10 column were collected and analyzed immediately.

Phosphorylation by ATP. DCC-NDPK (100 μM) was incubated with 1 mM ATP in 20 mM Tris-HCl (pH 8.0), 1 mM EDTA, and 0.6 mM $MgCl_2$ for 20 min at 37 °C. The protein was separated from nucleotide using a PD10 column equilibrated in 10 mM Tris-HCl (pH 8.0) and 1 mM EDTA. Typically, more than 90% of the protein in the eluate was phosphorylated. The phosphorylated protein was used either immediately or after storage on ice for up to 48 h. If necessary, the solution was concentrated using a microcentrifuge concentrator (Amicon) and could be stored at −80 °C.

Spectroscopic Measurements. Absorbance was measured on a Beckman DU640 spectrophotometer using cuvettes with a 1 cm path length. Fluorescence was recorded on a LS50B luminescence spectrometer from Perkin-Elmer with a xenon lamp and monochromator bandwidths set to 2.5 or 5 nm. Stopped-flow experiments used a HiTech SF61MX apparatus with a mercury−xenon lamp and HiTech IS-2 software. The monochromator for the excitation was set to 436 nm, and emission was recorded through a 455 nm cutoff filter. Solution concentrations are given in the figure legends as those in the mixing chamber. Mass spectrometry was performed as described previously (*4*). General data analysis was performed using the program Kaleidagraph (Synergy Software) and by Scientist (Micromath).

Analytical Ultracentrifugation. Sedimentation equilibrium centrifugation was carried out in a Beckman Optima XL-A analytical ultracentrifuge at 20 °C. DCC-NDPK (30 μM) in 10 mM Tris-HCl (pH 8.0) and 48 μM wild-type NDPK in 5 mM Tris-HCl (pH 8.2) and 0.1 mM EDTA were spun at 11 000, 16 000, and 25 000 rpm, the optimal speeds for a tetramer, dimer, and monomer, respectively. Absorbance was measured at 280 nm every hour until equilibrium was reached. The data were analyzed using the program Origin (MicroCal) by fitting to an ideal single-species model. A partial specific volume for NDPK of 0.746 mL/g, calculated from its amino acid sequence, and a monomeric molecular

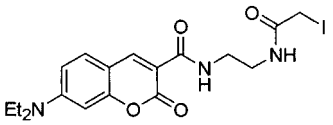

FIGURE 1: Structure of IDCC.

mass of 16 kDa were used in the analysis. The run at 11 000 rpm was repeated for a solution containing 10 μM DCC-NDPK, with absorbance monitored at 430 nm.

A second set of centrifugations was performed for the unphosphorylated labeled enzyme in the presence or absence of ADP and for the phosphorylated protein in the presence or absence of ATP. Protein concentrations were 9.8 and 3.9 μM for DCC-NDPK and 9.2 and 3.7 μM for DCC-NDPK∼P in 20 mM PIPES (pH 7.0), 50 μM EDTA, 30 μM $MgCl_2$, and 100 mM KCl. The runs were at a single speed (16 000 rpm) at 4 °C, and absorbance was measured at 440 nm.

RESULTS

Screening NDPK Mutants. To provide a specific attachment site for a fluorophore, a single cysteine was introduced at several defined positions in the NDPK molecule by oligonucleotide-directed mutagenesis. The sites of mutation were mainly on the protein surface near the nucleotide binding cleft. The single-cysteine mutants were purified and then labeled with a variety of thiol-reactive, environmentally sensitive fluorophores. These included several coumarin and dansyl fluorophores. Approximately 20 combinations of mutated enzymes and fluorophores were constructed, and most gave very small or no fluorescence changes upon addition of nucleotide. The protein with the best signal change has the single cysteine at position 112 ($NDPK^{D112C}$) labeled with a coumarin, *N*-[2-(iodoacetamido)ethyl]-7-diethylaminocoumarin-3-carboxamide (IDCC, Figure 1) (*24*). Other, closely related coumarin fluorophores attached to $NDPK^{D112C}$ gave very small fluorescence changes upon addition of nucleotide. The IDCC-labeled D112C protein is called DCC-NDPK below.

Fluorescence Labeling of $NDPK^{D112C}$ with IDCC. This labeling occurs rapidly and to 100%, indicating that the thiol group of Cys112 is easily accessible. Mass spectrometry of purified DCC-NDPK gave the expected mass (16 335.85 ± 0.64 Da), confirming a 1/1 labeling stoichiometry, and there was no indication of second-site labeling or unlabeled protein. Therefore, the absorbance spectrum of the coumarin could be used to determine the concentration of the labeled protein, and this value corresponds well with that from the colorimetric protein assay.

To determine whether the mutation and subsequent labeling had any effect on the oligomerization of NDPK, the molecular mass of DCC-NDPK was measured by sedimentation equilibrium ultracentrifugation. The data showed a complex with a molecular mass of 62.7 kDa, 4% lower than that calculated for a DCC-NDPK tetramer.

Fluorescence Properties of DCC-NDPK. The labeled protein has a 4-fold higher fluorescence in the presence of ATP than in the presence of ADP (Figure 2). We interpret this fluorescence change at low ATP concentrations as the phosphorylation of DCC-NDPK at His^{117}, with the phosphoenzyme (DCC-NDPK∼P) being the high-fluorescence state. There is a 6 nm red shift in the absorbance maximum

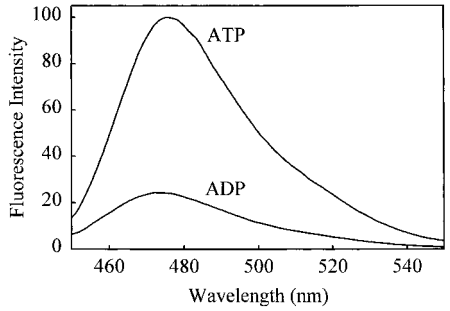

FIGURE 2: Fluorescence emission spectra of DCC-NDPK. Spectra were recorded at 20 °C for 2 μM DCC-NDPK in 20 mM PIPES (pH 7.0) and 2 mM $MgCl_2$ containing 50 μM ATP or 50 μM ADP. Excitation was at 441 nm.

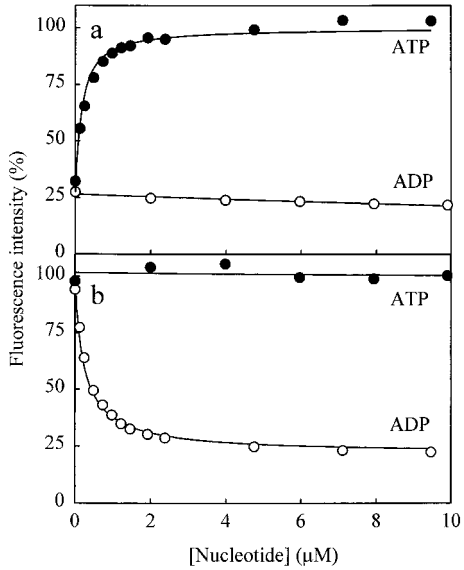

FIGURE 3: Titration of DCC-NDPK and DCC-NDPK∼P with ADP and ATP. A 200 μL solution containing 0.2 μM DCC-NDPK (a) or DCC-NDPK∼P (b) in 20 mM PIPES (pH 7.0) and 2 mM $MgCl_2$ was titrated at 20 °C with ATP or ADP. Nucleotide stock solutions contained $MgCl_2$ at a concentration 1.5 times greater than that of the nucleotide. Emission was recorded at 475 nm with excitation at 440 nm. The data were corrected for the small volume increases (<10%) and are presented as fluorescence percent of maximum. The solid lines represent the best global fit to the quadratic equations describing the equilibrium in eq 3 with a K_{eq} of 0.74 ± 0.14.

of the fluorophore between DCC-NDPK and DCC-NDPK∼P, with only a small decrease (12%) in the extinction coefficient. Fluorescence emission spectra obtained in the presence of GTP or GDP were virtually identical to those in Figure 2.

Fluorescence changes were measured on titration of DCC-NDPK with increasing concentrations of ADP and ATP (Figure 3a). The sensor showed a hyperbolic 4-fold increase in fluorescence with ATP, whereas ADP gave no significant fluorescence change in the same concentration range.

Phosphorylation of DCC-NDPK. To take advantage of the fluorescence change due to phosphorylation, DCC-NDPK was phosphorylated with ATP and then purified free of nucleotide. Mass spectrometry showed that this reaction had a yield of >90%, with the rest being mainly unphosphorylated DCC-NDPK. The fluorescent, phosphorylated enzyme (DCC-NDPK∼P) is stable on ice for at least 2 days with <5% dephosphorylation occurring and is stable at −80 °C for several months without significant dephosphorylation.

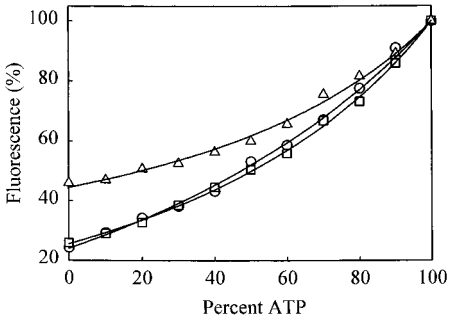

FIGURE 4: Dependence of fluorescence on the ADP/ATP concentration ratio. Fluorescence was measured as described in the legend of Figure 3 for 0.5 μM DCC-NDPK in the presence of different ADP/ATP concentration ratios, but at a fixed total nucleotide concentration. The titration was carried out at 10 μM (○), 100 μM (□), and 1 mM (△) total nucleotide. Fluorescence is shown as percentage of maximum. The curves are the best fit to an equation decribing the equilibrium in eq 3. The best-fit equilibrium constants are 0.58, 0.49, and 0.45, respectively. No correction was made for possible binding effects on fluorescence.

To test whether phosphorylation makes a difference to the oligomeric status of NDPK, a set of analytical ultracentrifugations was carried out either with the unphosphorylated DCC-NDPK in the presence or absence of ADP or with the phosphorylated enzyme in the presence or absence of ATP. In all cases, the data showed a complex between 61 and 69 kDa, consistent with a tetramer.

Fluorescence Properties of DCC-NDPK∼P. Titration of DCC-NDPK∼P with ADP (Figure 3b) showed a decrease to 25% in the fluorescence signal, whereas there was no significant change with ATP up to 100 μM. These data together with the results for the unphosphorylated sensor (Figure 3a) suggest that most of the signal change is due to dephosphorylation of DCC-NDPK∼P and that this change reflects the equilibrium between phosphorylated and unphosphorylated labeled protein (eq 3 where k_+ and k_- are the forward and reverse rate constants, respectively).

$$\text{ADP} + \text{DCC-NDPK}\sim\text{P} \underset{k_-}{\overset{k_+}{\rightleftharpoons}} \text{DCC-NDPK} + \text{ATP} \quad (3)$$

The titration data of DCC-NDPK with ATP and of DCC-NDPK∼P with ADP were fitted globally, giving an equilibrium constant K_{eq} (k_+/k_-) of 0.74. Because of this equilibrium, the ratio of phosphorylated to unphosphorylated protein, and therefore the fluorescence signal, is affected by the ATP/ADP concentration ratio. Thus, when 50 μM ADP is added to DCC-NDPK∼P, the full fluorescence change is observed. However, if this is repeated in the presence of 600 μM ATP, the fluorescence change is reduced to 25% of this maximum.

The fluorescence is also changed at high nucleotide concentrations, presumably by nucleotide binding: some combination of ADP binding to DCC-NDPK and ATP binding to DCC-NDPK∼P. This is illustrated in Figure 4 which shows how the fluorescence depends on the ADP/ATP concentration ratio at a fixed total nucleotide concentration. At 10 and 100 μM total nucleotide, the curves are indistinguishable. At 1 mM, the response is reduced, but there is still a clear dependence of fluorescence on the ADP/ATP concentration ratio.

The fluorescence quantum yields of DCC-NDPK∼P and DCC-NDPK were determined using the known value (0.83) for Coumarin 314 in ethanol (*31*) as a reference. There was a 4-fold increase in the quantum yield when going from the unphosphorylated sensor (0.054) to the phosphorylated (0.22), in good agreement with the observed levels of fluorescence emission of DCC-NDPK in the presence of ATP or ADP (Figure 2).

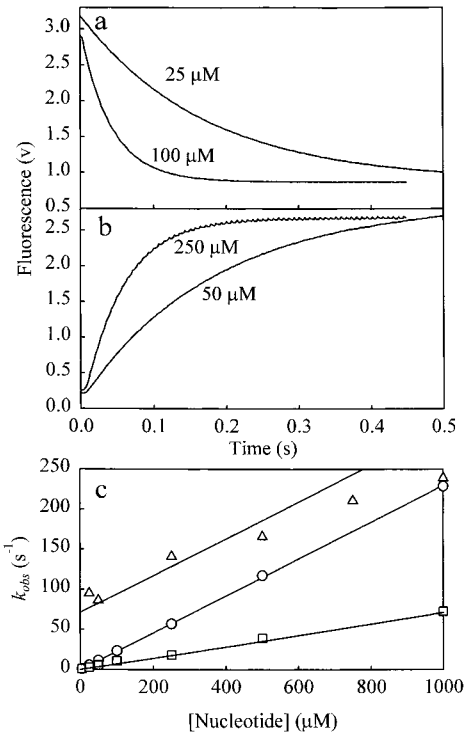

FIGURE 5: Transient kinetics of ADP and ATP interaction with DCC-NDPK. Fluorescence stopped-flow measurements were carried out in 20 mM PIPES (pH 7.0) and 2 mM $MgCl_2$ at 20 °C. All concentrations given are those in the mixing chamber. (a) ADP (25 or 100 μM) was mixed with 1 μM DCC-NDPK∼P. The curves were fitted to single exponentials giving k_{obs} values of 5.7 and 23.9 s^{-1}. (b) ATP (50 or 250 μM) was mixed with 1 μM DCC-NDPK. The curves were fit to a single exponential giving observed rate constants k_{obs} of 5.5 and 18.5 s^{-1}. (c) k_{obs} values are plotted vs the concentration of ADP (○) or ATP (□). The solid lines show the best linear fit with second-order rate constants of 2.3×10^5 (ADP) and 0.71×10^5 M^{-1} s^{-1} (ATP) from the slope. The triangles show the observed rate constants when ADP was mixed with DCC-NDPK∼P in the presence of 1 mM ATP. The line is the predicted dependence from eqs 3 and 6; the intercept is at 71 s^{-1} ($=0.71 \times 10^5$ M^{-1} s^{-1} $\times$ 1 mM), and the slope is 2.3×10^5 M^{-1} s^{-1}. The deviation at high ADP concentrations may be due to ATP bound to DCC-NDPK∼P with its release being partially rate limiting (see the text).

Kinetic Measurements. Three types of transient kinetic measurements were carried out using a fluorescence stopped-flow apparatus. First, the rate of dephosphorylation of DCC-NDPK∼P was measured over a range of ADP concentrations (Figure 5a). The observed rate constants increased linearly with increasing nucleotide concentrations, and a second-order rate constant was calculated from the slope of the linear fit, giving a value of 2.3×10^5 M^{-1} s^{-1} (Figure 5c). A similar measurement was performed for the phosphorylation of DCC-NDPK with ATP (Figure 5b). Again, there was a linear increase in the rates with increasing ATP concentrations, and the deduced second-order rate constant was 0.71×10^5 M^{-1} s^{-1} (Figure 5c). Finally, in the third measurement, the rate of dephosphorylation was measured in the presence of 1 mM ATP. The observed dephosphorylation rates were higher in

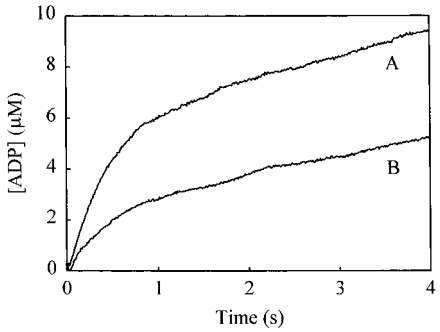

FIGURE 6: ADP release from rabbit skeletal myosin subfragment 1 (S1). Fluorescence emission was recorded on mixing 1 μM DCC-NDPK∼P and 100 μM ATP with a 25 μM S1/10 μM ADP mixture in 20 mM PIPES (pH 7.0) and 2 mM $MgCl_2$ at 20 °C (A). The fluorescence change was also measured with 5 μM ADP (B). The fluorescence signal was calibrated by replacing S1 with 5 or 10 μM ADP to give the amount of ADP released. The data were fitted to a single-exponential plus linear equation, yielding rate constants of 2.4 (5 μM ADP) and 2.5 s^{-1} (10 μM ADP) for the exponential phase and slopes of 0.73 (5 μM) and 0.96 μM s^{-1} (10 μM) for the slow, linear phase. The slope values were divided by S1 concentration, resulting in steady-state k_{cat} values of 0.03 (5 μM) and 0.04 s^{-1} (10 μM).

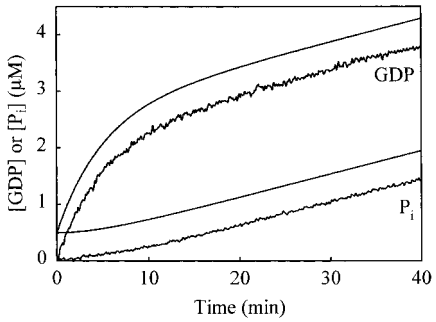

FIGURE 7: GDP and P_i release from human rho. Fluorescence emission was recorded for a 200 μL solution at 30 °C containing 20 mM Tris-HCl (pH 7.6), 1 mM $MgCl_2$, 100 mM $(NH_4)_2SO_4$, 10 μM GTP, and either 2 μM DCC-NDPK∼P (for GDP measurement) or 10 μM MDCC-PBP (for P_i). Reactions were started by adding 2 μM rho·GDP. Excitation was at 440 (GDP) or 430 nm (P_i) with the emission measured at 475 or 465 nm, respectively. The GDP data were calibrated using the fluorescence change on adding 1 μM GDP to DCC-NDPK∼P with different GTP/GDP concentration ratios. The P_i data were calibrated by adding different concentrations of P_i to MDCC-PBP. The two sets of data were fitted globally to the single-exponential plus linear equation for the two-step scheme (eqs 4 and 5), giving rate constants of 3.1×10^{-3} s^{-1} for GDP release and 3.0×10^{-4} s^{-1} for hydrolysis. Theoretical lines are shown offset by 0.5 μM for clarity.

the presence of ATP than in its absence (Figure 5c). These results will be interpreted in the Discussion in terms of the simple model in eq 3 so that the observed rate constants are the sum of the rate constants for phosphorylation and dephosphorylation.

An equivalent set of measurements was carried out with GDP and GTP. The second-order rate constants are 0.91×10^5 M^{-1} s^{-1} for dephosphorylation and 0.50×10^5 M^{-1} s^{-1} for phosphorylation.

ADP Release from Myosin Subfragment 1. To test the novel diphosphate sensor, two different NTPase reactions were studied. First, release of ADP was assessed from subfragment 1 (S1), a proteolytic fragment of myosin which contains the ATPase catalytic site. The data were obtained in a stopped-flow apparatus by mixing DCC-NDPK∼P and ATP with the S1·ADP complex at two different ADP concentrations and following the displacement of ADP from the complex during the first few turnovers of the ATPase (Figure 6). The release during the first turnover was fitted to an exponential with rate constants of 2.4 and 2.5 s^{-1}, in good agreement with previously measured values [e.g., 2.4 s^{-1} (*32*)]. During subsequent turnovers, ADP was released at a rate governed by the steady-state rate of the ATPase. The rate constant for this phase (0.03−0.04 s^{-1}) is constant over a range of NDPK concentrations and within the range of previously determined values.

In the absence of S1, an exponential change in fluorescence was observed with a rate constant of 8.0 s^{-1} at 2 μM ADP (data not shown), indicating that the signal with S1 is mostly determined by ADP release.

Kinetics of GDP Release from Rho. A second test for the sensor was the release of GDP from rho, a well-characterized member of the ras superfamily of small GTPases. GDP release and steady state GTPase activity were measured using the diphosphate sensor and results compared with those obtained by alternative methods. Small G proteins such as rho contain a tightly bound GDP in the catalytic site. Removal of this nucleotide is accelerated in vivo by protein exchange factors (GEFs) and but can be achieved in vitro by lowering the Mg^{2+} concentration with EDTA and/or by addition of ammonium sulfate (*33*). GDP release in this system has previously been assessed using the nucleotide analogue mantGDP, which changes fluorescence on release from rho (*34*). The reaction scheme is

$$\text{Rho·GDP} + \text{GTP} \rightleftharpoons \text{Rho·GTP} + \text{GDP} \quad (4)$$

$$\text{Rho·GTP} \rightarrow \text{Rho·GDP} + P_i \quad (5)$$

The rate of the first process is limited by GDP release, and this step was made essentially irreversible by the excess of GTP and the removal of GDP by DCC-NDPK. P_i release during GTP hydrolysis was assessed using the P_i sensor, MDCC-PBP (*3*). To accelerate GDP release, 100 mM ammonium sulfate was present. The data obtained with the diphosphate and P_i sensors are shown in Figure 7. The rate constant for exponential release of GDP during the first turnover, detected by DCC-NDPK∼P, corresponds well to the lag phase in the P_i trace, and both traces show the same steady state, as demonstrated by the good global fit to the two sets of data. The rate constants agree well with the equivalent rate constant of GDP release determined using mantGDP (data not shown).

DISCUSSION

NDPK was developed as a specific sensor for nucleoside diphosphates by labeling the protein with a coumarin fluorophore, IDCC. In using the phosphorylated protein, we took advantage of the following facts. First, this phosphoenzyme has a high fluorescence compared with the unphosphorylated protein. Second, the phosphoenzyme is stable over the time range needed for its preparation and subsequently for monitoring kinetic events such as the release of ADP from an ATPase. Finally and most importantly, the phosphorylation allows the sensor to discriminate between NDP which causes a large fluorescence change and NTP which does not alter the signal because the basis for the signal

change is dephosphorylation (eq 3). The sensor measures the NDP/NTP concentration ratio and so can detect small quantities of NDP in the presence of much higher concentrations of NTP. This is important, for example, in experiments in single muscle fibers where initial ATP concentrations are high (*2*) but also more generally for measurements in cytosolic extracts.

Mechanism. Transient kinetic methods have been used to measure the rate constants for ADP binding leading to dephosphorylation, 2.1×10^5 M^{-1} s^{-1}, and ATP binding leading to phosphorylation, 0.7×10^5 M^{-1} s^{-1} (20 °C). Over the range of concentrations that was studied, the observed rate increased linearly with nucleotide concentration. It follows that the dephosphorylation step itself must be >200 s^{-1} (the maximum rate observed) and that nucleotide binding to the protein is weak (see below).

The comparatively slow rate of dephosphorylation at low ADP concentrations is significantly accelerated when ATP is present (Figure 5c), although the intensity of the ADP-induced fluorescence change is reduced. This is predicted because the sensor monitors the equilibrium between its phosphorylated and unphosphorylated forms (eq 3). This model predicts that the observed rate constant and intensity change are given by

$$k_{obs} = k_+[ADP] + k_-[ATP] \quad (6)$$

$$\Delta\text{fluorescence} = \Delta\text{fluorescence}_{max}[ADP]/(K_{eq}[ATP] + [ADP]) \quad (7)$$

where $\Delta\text{fluorescence}_{max}$ is the fluorescence change at 0 M ATP. These equations seem to hold, at least at low nucleotide concentrations. At higher nucleotide concentrations, binding may become important and these equations have been considered for human NDPK (*35*).

Transient kinetic data obtained for the dephosphorylation of human NDPK A (*35*) show that the apparent second-order rate constant of ADP binding is 50 times higher than that for DCC-NDPK∼P. For the phosphorylation rate constants (DCC-NDPK plus ATP), the difference is almost 100-fold. The sequences of the *M. xanthus* and human proteins differ slightly, but the steady-state parameters (K_m and k_{cat}) are similar. So it seems more likely that the reduced activity is due to the mutation or the attached fluorophore or a combination of these.

A titration of fluorescence versus nucleotide concentration gives an equilibrium constant for eq 3 (K_{eq}) of 0.74. The ratio of rate constants, k_+/k_-, will equal K_{eq} if eq 3 fully holds. This ratio is 0.31 with ADP and ATP and 0.55 with GTP and GDP. Clearly, eq 3 is a simplification as it ignores binding (and release) of nucleotides as a separate step, and this becomes significant at high nucleotide concentrations (see below). However, the equilibrium constant between phosphorylated and unphosphorylated forms is close to unity, so the fluorescence changes over a wide range of nucleotide ratios.

Use as a Sensor. The low specificity of the nucleotide binding site of NDPK with respect to purine allows the sensor to be used for measuring the amount of GDP as well as ADP. Both nucleotides give the same fluorescence change and similar rates for dephosphorylation of DCC-NDPK∼P. As an example, the release of GDP from rho was assessed and is discussed later. Because the fluorescence responds to the NDP/NTP concentration ratio, DCC-NDPK can also be used to monitor ATP or GTP formation in the presence of the diphosphate. However, it should be noted that because the diphosphate sensor does not discriminate between ADP and GDP, it will not measure changes of ADP when GDP is also changing: it will measure the sum change.

Because the fluorescence intensity is primarily determined by the phosphorylation state and nucleotide binding is weak, eq 3 is sufficient to explain most of the results quantitatively. At high nucleotide concentrations (>100 μM), there are secondary effects due to the presence of protein·nucleotide complexes, and these will become significant at millimolar concentrations (Figure 4). An example is also seen in Figure 5c, where 1 mM ATP causes an increase in the observed rate constant for ADP's interaction with DCC-NDPK∼P. The data fit the model for eq 3 at low concentrations, but deviate at high. There are secondary effects due to binding observed in titration data as in Figure 2. Millimolar concentrations of ADP cause a small rise in fluorescence when added to unphosphorylated DCC-NDPK, presumably because the DCC-NDPK·ADP complex has a fluorescence different from that of the apoprotein.

Where the DCC-NDPK∼P concentration is very low and no extraneous ATP is present, the sensor is sensitive at submicromolar ADP concentrations (Figure 3). The sensor can measure down to ∼10 nM ADP under these conditions. In contrast, where the ATP concentration is in the millimolar range, then the sensor is most sensitive in the hundred micromolar to millimolar range of ADP concentrations. As for all fluorescence-based assays, a calibration is required for the particular experimental conditions.

The measurement of kinetics descibed here (Figure 5) indicates the limitations for measuring rates of diphosphate formation. There is a trade-off of sensitivity versus rate, as the rate of dephosphorylation is greatly increased by the presence of triphosphate, but the fluorescence change is decreased. Thus, >80 s^{-1} rates are observed when 1 mM ATP is present, but signal-to-noise considerations mean that the sensitivity is ∼10 μM ADP (1% of total nucleotide concentration) when a 4% fluorescence change is expected. The rate can also be increased by increasing the concentration of the sensor, as the main limitation of dephosphorylation rate is the bimolecular rate constant.

A major alternative assay for ADP is provided by a coupled enzyme approach, particularly using pyruvate kinase and lactate dehydrogenase and monitoring NADH oxidation by absorbance or fluorescence. This typically can measure in the micromolar range. It is rapid when substrates are saturating, but the multiple components and low K_m for some of the substrates mean that it is difficult to achieve clean coupling to the reaction of interest that forms ADP. For example, significant lags may be observed.

The sensor was tested with measurements on two systems for which rate constants could be obtained by other methods: ADP release from myosin and GDP release from rho. In both cases, the results are similar to those expected for the release rate constant and for the subsequent steady-state hydrolysis. The measurement of the amounts of P_i and GDP for rho illustrates the complementarity of the diphosphate and P_i sensors. In the steady state, they give similar information (the GTPase rate), but in the approach to steady

state in this case, the burst phase of GDP release is matched by a lag in P_i.

In summary, we have developed a new fluorescence sensor for NDP or NTP based on nucleoside diphosphate kinase that is sensitive for NDP both in the absence and in the presence of NTP. This was achieved by engineering a fluorophore-labeled protein that occupies a high fluorescence state when phosphorylated (DCC-NDPK∼P) and a low fluorescence state when in its unphosphorylated form (DCC-NDPK). The sensor should be suitable for a wide range of biological systems.

ACKNOWLEDGMENT

We thank Dr. R. Williams (Cambridge University) for the gift of plasmid pJM5C2A, Mrs. J. Hunter (National Institute for Medical Research) for preparing myosin subfragment 1, and Dr. J. Hutchinson (National Institute for Medical Research) for rho protein. We thank Mr. G. Bonifacio, Ms. S. Major, and Dr. J. F. Eccleston (National Institute for Medical Research) for making the analytical ultracentrifuge measurements and Mr. S. A. Howell (National Institute for Medical Research) for making the mass spectral measurements.

REFERENCES

1. Hibberd, M. G., and Trentham, D. R. (1986) *Annu. Rev. Biophys. Biophys. Chem. 15*, 119−161.
2. He, Z. H., Chillingworth, R. K., Brune, M., Corrie, J. E. T., Trentham, D. R., Webb, M. R., and Ferenczi, M. A. (1997) *J. Physiol. 501*, 125−148.
3. Brune, M., Hunter, J. L., Corrie, J. E. T., and Webb, M. R. (1994) *Biochemistry 33*, 8262−8271.
4. Brune, M., Hunter, J. L., Howell, S. A., Martin, S. R., Hazlett, T. L., Corrie, J. E. T., and Webb, M. R. (1998) *Biochemistry 37*, 10370−10380.
5. Barman, T., Brune, M., Lionne, C., Piroddi, N., Poggesi, C., Stehle, R., Tesi, C., Travers, F., and Webb, M. R. (1998) *Biophys. J. 74*, 3120−3130.
6. Gilbert, S. P., Webb, M. R., Brune, M., and Johnson, K. A. (1995) *Nature 373*, 671−676.
7. Lowe, D. J., Ashby, G. A., Brune, M., Knights, H., Webb, M. R., and Thorneley, R. N. F. (1995) in *Nitrogen fixation: fundamentals and applications* (Tikhonovich, I. A., Ed.) pp 103−108, Kluwer Academic Publishers, Dordrecht, The Netherlands.
8. Dillingham, M. S., Wigley, D. B., and Webb, M. R. (2000) *Biochemistry 39*, 205−212.
9. Parks, R. E., and Agarwal, R. P. (1972) in *The Enzymes* (Boyer, P. D., Ed.) pp 483−514, Academic Press, New York.
10. Wålinder, O., Zetterqvist, Ö., and Engström, L. (1968) *J. Biol. Chem. 244*, 1060−1064.
11. Lascu, I., Schaertl, S., Wang, C., Sarger, C., Giartosio, A., Briand, G., Lacombe, M.-L., and Konrad, M. (1997) *J. Biol. Chem. 272*, 15599−15602.
12. De la Rosa, A., Williams, R. L., and Steeg, P. S. (1995) *BioEssays 17*, 53−62.
13. Chakrabarty, A. M. (1998) *Mol. Microbiol. 28*, 875−882.
14. Dumas, C., Lascu, I., Morera, S., Glaser, P., Fourme, R., Wallet, V., Lacombe, M., Veron, M., and Janin, J. (1992) *EMBO J. 11*, 3203−3208.
15. Williams, R. L., Oren, D. A., Munoz-Dorado, J., Inouye, M., and Arnold, E. (1993) *J. Mol. Biol. 234*, 1230−1247.
16. Morera, S., Chiadmi, M., LeBras, G., Lascu, I., and Janin, J. (1995) *Biochemistry 34*, 11062−11070.
17. Webb, P. A., Perisic, O., Mendola, C. E., Backer, J. M., and Williams, R. L. (1995) *J. Mol. Biol. 251*, 574−587.
18. Hama, H., Almaula, N., Lerner, C. G., Inouye, S., and Inouye, M. (1991) *Gene 105*, 31−36.
19. Munoz-Dorado, J., Inouye, M., and Inouye, S. (1990) *J. Biol. Chem. 265*, 2702−2706.
20. Munoz-Dorado, J., Inouye, S., and Inouye, M. (1990) *J. Biol. Chem. 265*, 2707−2712.
21. Gibson, T. J. (1984) Studies on the Epstein−Barr virus genome, Ph.D. Thesis, Cambridge University, Cambridge, England.
22. Hanahan, D. (1983) *J. Mol. Biol. 166*, 557−580.
23. Weeds, A. G., and Taylor, R. S. (1975) *Nature 257*, 54−56.
24. Corrie, J. E. T. (1994) *J. Chem. Soc., Perkin Trans. 1*, 2975−2982.
25. Olsen, D. B., Sayers, J. R., and Eckstein, F. (1993) in *Methods in Enzymology* (Wu, R., Ed.) Vol. 217, Recombinant DNA, Part H, pp 189−217, Academic Press, London.
26. Sambrook, J., Fritsch, E. F., and Maniatis, T. (1989) *Molecular cloning. A laboratory manual*, 2nd ed., Cold Spring Harbor Laboratory Press, Cold Spring Harbor, NY.
27. Postel, E. H., Berberich, S. J., Flint, S. J., and Ferrone, C. A. (1993) *Science 261*, 478−480.
28. Mesnildrey, S., Agou, F., and Véron, M. (1997) *FEBS Lett. 418*, 53−57.
29. Gill, S. C., and von Hippel, P. H. (1989) *Anal. Biochem. 182*, 319−326.
30. Almaula, N., Lu, Q., Delgado, J., Belkin, S., and Inouye, M. (1995) *J. Bacteriol. 177*, 2524−2529.
31. Fletcher, A. N., and Bliss, D. E. (1978) *Appl. Phys. 16*, 289−295.
32. Marston, S. B., and Taylor, E. W. (1980) *J. Mol. Biol. 139*, 573−600.
33. Hoshino, M., Clanton, D. J., Shih, T. Y., Kawakita, M., and Hattori, S. (1987) *J. Biochem. 102*, 503−511.
34. Hutchinson, J. P., and Eccleston, J. F. (2000) *Biochemistry 39*, 11348−11359.
35. Schaertl, S., Konrad, M., and Geeves, M. A. (1998) *J. Biol. Chem. 273*, 5662−5669.

BI002484H